Electronic Supplementary Material (ESI) for Lab on a Chip.

Supplementary Information

Real-time spectroscopic monitoring of continuous synthesis of zinc oxide nanostructures in femtosecond laser fabricated 3D microfluidic microchannels with integrated on-chip fiber probe array

Miao Wu,[a, b] Xin Li,[a*] Di-Feng Yin,[c] Wei Chen,[a, b] Jia Qi,[a, b] Ming Hu,[a] Jian Xu,[a, b] and Ya Cheng[a, b, c] **[*]

a State Key Laboratory of Precision Spectroscopy, Engineering Research Center for Nanophotonics &Advanced Instrument, Ministry of Education, School of Physics and Electronic Science, East China Normal University, Shanghai, 200241, China

b XXL –The Extreme Optoelectromechanics Laboratory, School of Physics and Electronic Science, East China Normal University, Shanghai, 200241, China

c State Key Laboratory of High Field Laser Physics and CAS Center for Excellence in Ultra-intense Laser Science, Shanghai Institute of Optics and Fine Mechanics (SIOM), Chinese Academy of Sciences (CAS), Shanghai, 201800, China

---

[*] Corresponding author: xli@phy.ecnu.edu.cn, ya.cheng@siom.ac.cn

Configuration of the concentration gradient (CGGs)

This concentration gradient module aimed to establish five independent concentration conditions for each reactor. This module consists of two Christmas tree-shaped concentration gradient generators (CGGs), independently in two horizontal layers ahead of the reaction module, each with 3D mixers of a unit size of 2 × 1 mm^2. The two CGGs have a size of 7.2 × 9.8 cm^2 each and are located independently in two horizontal layers ahead of the reaction module. The perfused solutions flow through the CGGs and automatically split at bifurcation points to generate outflows with variable concentrations, which can be favorable for screening synthetic parameters of ZnO later. Compared to conventional serpentine microchannels in the CGGs, the 3D mixers designed using Baker's transformation can repeatedly split the fluid into microstreams and reorganize them. The mixers have been shown to possess high mixing efficiency without compromising the flux while being able to handle flow rates between 5 and 100 mL min^{-1}.

Simulation and analysis of concentration gradient

Table S1 The parameters of flow dynamics.

Flow rate (mL/min)	5	12.5	25	50
U (m/s)	0.083	0.208	0.417	0.833
Re	83	208	417	833

The governing equations of fluid flow in microfluidic chip channels can be derived from the conservation of mass and conservation of momentum, which are called the continuity equation and Navier-Stokes equation respectively. In the model, it is assumed that the flow state in the microfluidic chip channel is a laminar flow state and steady state, and the internal fluid is an incompressible Newtonian fluid. For incompressible Newtonian fluids, the above equation can be described as:

Equation of continuity:

$$\nabla \times v = 0$$

Momentum equation:

$$\rho\frac{\partial v}{\partial t}+\rho(v\cdot\nabla)v=-\nabla P+\mu\nabla^2 v$$

where v represents the velocity vector, ρ represents the fluid density, μ represents the dynamic viscosity of the fluid, and P represents the constant temperature pressure. The simulated fluid is set to water, with a viscosity of 1×10^{-3} N*s/m^2, and a density of 1000 kg/m^3.

Fluid mixing in microfluidic chip channels is mainly controlled by the law of conservation of matter, which is given by the convection and diffusion equation, whose equation can be described as:

Species convection and diffusion equation:

$$\frac{\partial c}{\partial t}+v\cdot\nabla c=D\nabla^2 c$$

c represents the solute concentration; D represents the species diffusion coefficient.

The setting of boundary conditions: at the entrance, the model assumes a fully developed laminar flow, and the velocity of the two entrances is the same as v.

To quantitatively evaluate the mixing efficiency of microfluidic chips I, the formula for calculating the mixing efficiency at any cross-section in the mixing channel is defined as:

$$I=\left(1-\sqrt{\frac{\sigma_m^2}{\sigma_{max}^2}}\right)\times 100\%$$

$$\sigma_m^2=\frac{1}{N}\sum_{i=0}^{N}(c_i-\bar{c})^2$$

where N is the total number of a cross-section grid cell, c_i is each grid cell mass concentration, with $\bar{c}$ is c_i for cross-section calculation of average, σ_{max}^2 is the maximum variance of mixture concentration along each cross-section of the channel (that is, the variance of concentration when there is no mixing at the entrance). σ_{max}^2 is calculated by the following formula:

$$\sigma_{max}^2=\bar{c}(1-\bar{c})$$

The value of mixing efficiency I varies from 0 (no mixing) to 100% (full mixing).

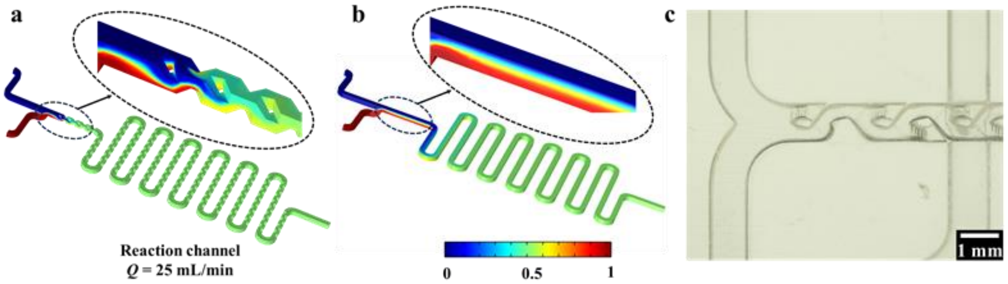

Fig. S1 (a) Numerical simulation results of concentration distribution in the reaction channels when the inlet flow rate Q was 25 mL min^{-1}. (b) Numerical simulation results of concentration distribution in conventional serpentine microchannels when the inlet flow rate Q was 25 mL min^{-1}. (c) Photograph of the mixing units on chip.

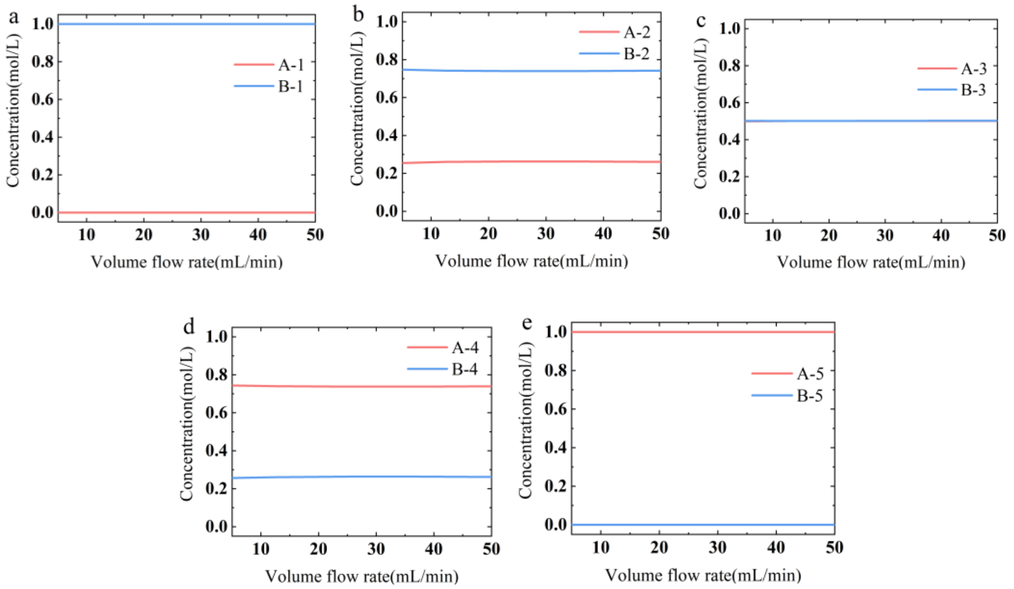

Fig.S2 Concentrations of the fluids at outlets before entering the reaction module at different flow rates.

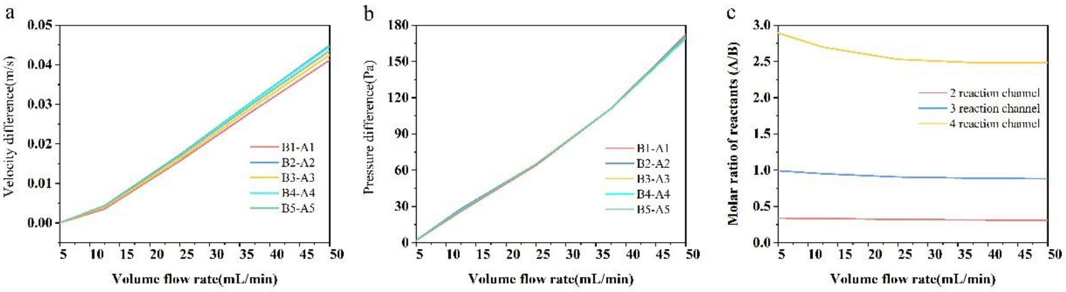

Fig. S3 Numerical simulation results at the outlet ahead of the reaction module at different flow rates. (a) Velocity difference. (b) Pressure difference. (c) Molar ratio.

In this work, two kinds of fluid were simulated, one with solute, and the other without solute, to facilitate normalization. The fluids at the outlets which are named A1 to A5 in the lower layer and B1 to B5 in the upper layer show different colors, indicating a concentration gradient interval of approximately 25%. The outlets were subsequently mixed in the reaction module. The uniform color shown in the reaction channel has an obvious mixing effect, realizing complete mixing quickly after entering.

In microfluidic flow synthesis, the flow rate is an important synthetic parameter that can determine the molar ratio of matter and may influence the reaction kinetics. Therefore, we use numerical simulation to consider the influence of the flow rate on the concentration gradient, the velocity difference, and the pressure difference at the two entrances of each reactor. Fig. S2 shows that the concentration gradient was almost steady in a range of flow rates from 5 to 50 mL min^{-1}. Fig. S3a presents that the velocity difference at the two entrances of each reactor gradually increased with the flow rate. This is probably caused by the increased pressure difference as shown in Fig. S3b. The molar ratios of substances in channels 2, 3, and 4 were calculated, respectively (Fig. S3c). With the increase in the flow rate, the molar ratio in all three reaction channels showed a downward trend and eventually stabilized. The absence of any crossing of molar ratios indicates that the reaction conditions remained in a step distribution. Therefore, in the following case experiments, the reactions are all carried out in stepped-distribution conditions within the range of the flow rate tested. Besides, within this range, slight variations in velocity and pressure difference can be observed. The averaged spectra were collected over a short integration time of 10 ms. Such short integration time allows for precise real-time monitoring. The final spectral analysis was obtained by averaging over five individual tests for each sample point. This approach helps eliminate the impact of flow fluctuations and ensures the stability of the detection process.

Validation functions of the microfluidic flow synthesizer

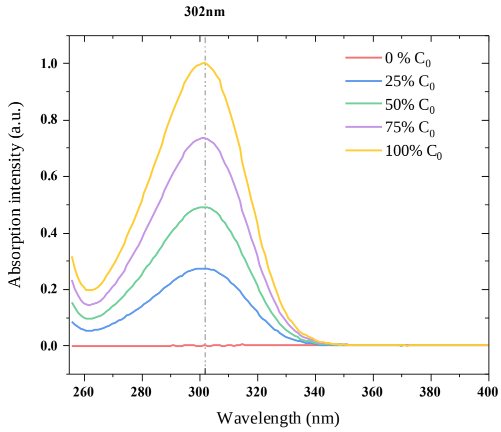

Fig. S4 Ultraviolet-visible absorption spectrum of zinc nitrate solution measured by a commercial UV-2600 photo spectrometer. C_0 represents the initial concentration of $Zn(NO_3)_2$.

After the numerical simulation study, we use an online monitoring module to collect experimental data to verify the gradient concentration in the reactors and check whether the online monitoring module can work properly. Here zinc nitrate solution of a concentration of 300 mM was loaded into the channel via inlets A and B, and deionized (DI) water was loaded via the other two inlets with a flow rate of 12.5 mL min^{-1}.

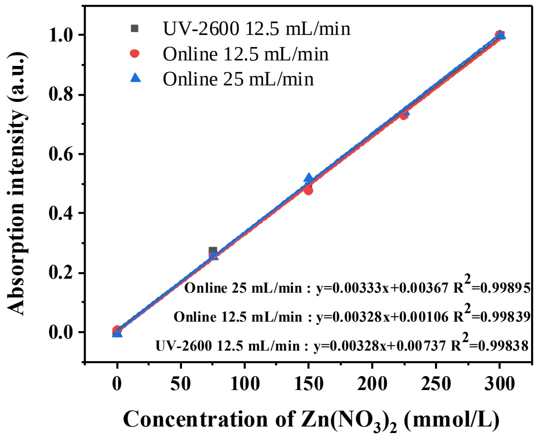

Fig. S5 Correlation between the concentration of $Zn(NO_3)_2$ and the peak intensity as measured by an online monitoring module and a commercial UV-2600 spectrometer.

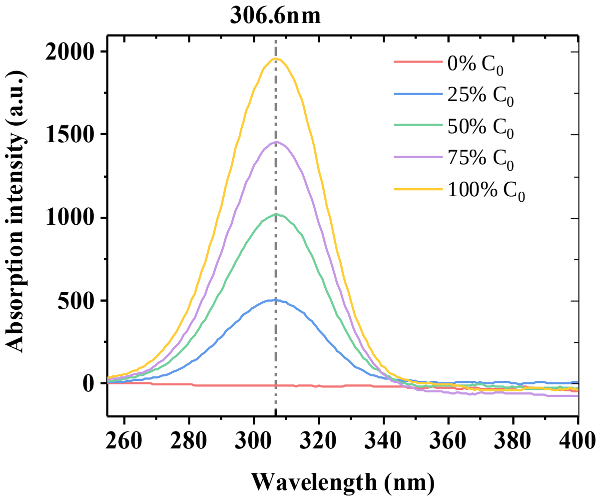

Fig. S6 Online spectra taken at the microcells when the inlet flow rate *Q* was 25 mL min^{-1}. C_0 represents the initial concentration of $Zn(NO_3)$.

We extracted the peak intensities of the online spectra and analysed the relationship between the peak intensities and the calculated concentration of the $Zn(NO_3)_2$ in the microcells by assuming that the concentration gradient with a gradient interval of approximately 25% was established in the microcells. A linear relationship that was very similar to the calibration curve was observed in Fig. S5, confirming the generation of the concentration gradient and the accuracy and the high spatial resolution of the online spectra. In addition, when the flow rate was increased to 25 mL min^{-1}, the online spectra presented a very close linear relationship between the concentration of the $Zn(NO_3)_2$ and the peak intensity (with a coefficient R2 of 0.99 again) (Fig. S5 and S6). Therefore, the online monitoring module can work properly under varied flow rates in the reactors. Upon the perfusion of the $Zn(NO_3)_2$ solution into the microchannel at a flow rate of 25 mL min^{-1}, we observed the rapid variation in concentration as it reached each microcell (Fig. S7). This real-time monitoring allowed us to capture the dynamic changes in concentration with high temporal resolution, providing valuable insights into the synthesis process. The ability to track concentration variations at such a high temporal resolution is an essential advantage of our on-chip monitoring system.

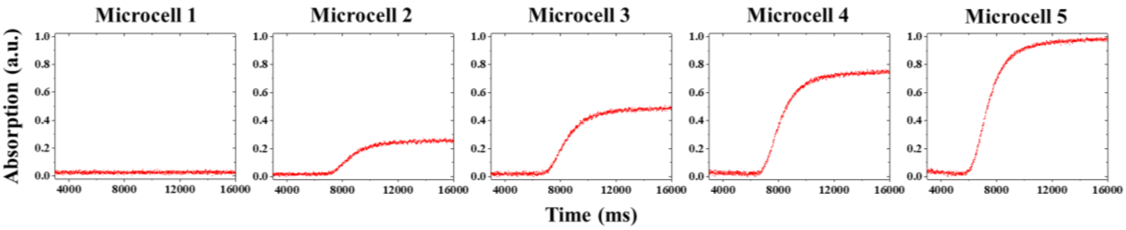

Fig. S7 Absorption spectra collected from five microcells as a function of time with the flow rate of 25 mL min^{-1}.

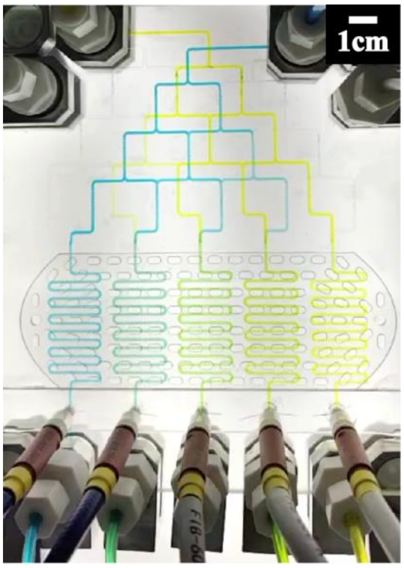

Fig. S8 Demonstration of the homogeneous mixing in the glass device

To further demonstrate the homogeneous mixing of solutions in the glass device, blue and yellow dye solutions were used for mixing with the flow rate of 25 mL min^{-1} (Fig. S8).

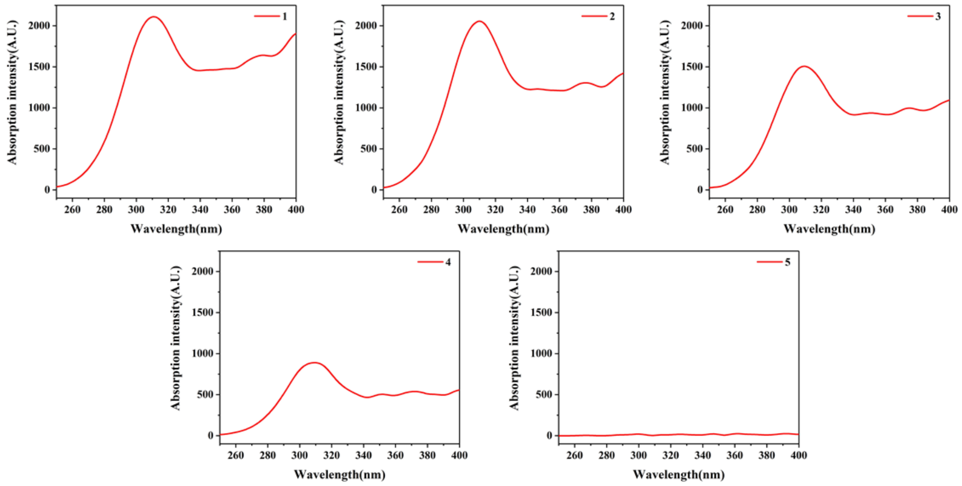

Fig. S9 Online spectra of the synthesized products obtained under room temperature with a fluidic rate of 12.5 mL/min.

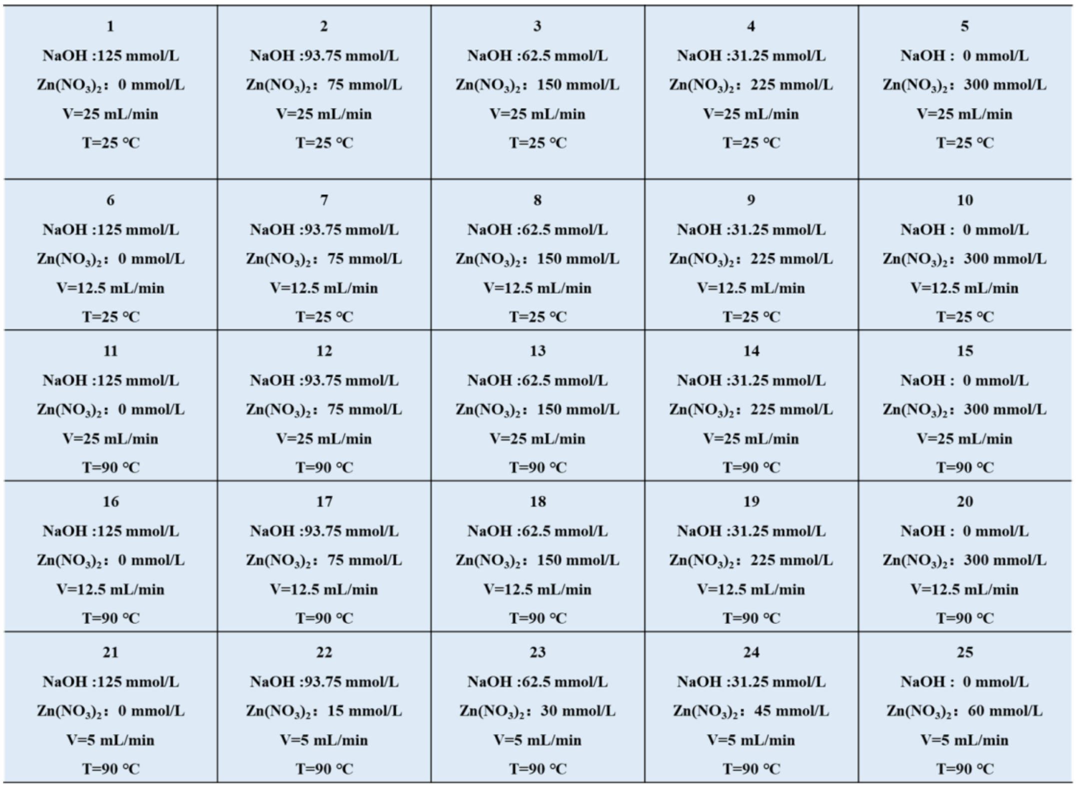

1 **NaOH :125 mmol/L** **$Zn(NO_3)_2$： 0 mmol/L** **V=25 mL/min** **T=25 °C**	**2** **NaOH :93.75 mmol/L** **$Zn(NO_3)_2$： 75 mmol/L** **V=25 mL/min** **T=25 °C**	**3** **NaOH :62.5 mmol/L** **$Zn(NO_3)_2$： 150 mmol/L** **V=25 mL/min** **T=25 °C**	**4** **NaOH :31.25 mmol/L** **$Zn(NO_3)_2$： 225 mmol/L** **V=25 mL/min** **T=25 °C**	**5** **NaOH : 0 mmol/L** **$Zn(NO_3)_2$： 300 mmol/L** **V=25 mL/min** **T=25 °C**
6 **NaOH :125 mmol/L** **$Zn(NO_3)_2$： 0 mmol/L** **V=12.5 mL/min** **T=25 °C**	**7** **NaOH :93.75 mmol/L** **$Zn(NO_3)_2$： 75 mmol/L** **V=12.5 mL/min** **T=25 °C**	**8** **NaOH :62.5 mmol/L** **$Zn(NO_3)_2$： 150 mmol/L** **V=12.5 mL/min** **T=25 °C**	**9** **NaOH :31.25 mmol/L** **$Zn(NO_3)_2$： 225 mmol/L** **V=12.5 mL/min** **T=25 °C**	**10** **NaOH : 0 mmol/L** **$Zn(NO_3)_2$： 300 mmol/L** **V=12.5 mL/min** **T=25 °C**
11 **NaOH :125 mmol/L** **$Zn(NO_3)_2$： 0 mmol/L** **V=25 mL/min** **T=90 °C**	**12** **NaOH :93.75 mmol/L** **$Zn(NO_3)_2$： 75 mmol/L** **V=25 mL/min** **T=90 °C**	**13** **NaOH :62.5 mmol/L** **$Zn(NO_3)_2$： 150 mmol/L** **V=25 mL/min** **T=90 °C**	**14** **NaOH :31.25 mmol/L** **$Zn(NO_3)_2$： 225 mmol/L** **V=25 mL/min** **T=90 °C**	**15** **NaOH : 0 mmol/L** **$Zn(NO_3)_2$： 300 mmol/L** **V=25 mL/min** **T=90 °C**
16 **NaOH :125 mmol/L** **$Zn(NO_3)_2$： 0 mmol/L** **V=12.5 mL/min** **T=90 °C**	**17** **NaOH :93.75 mmol/L** **$Zn(NO_3)_2$： 75 mmol/L** **V=12.5 mL/min** **T=90 °C**	**18** **NaOH :62.5 mmol/L** **$Zn(NO_3)_2$： 150 mmol/L** **V=12.5 mL/min** **T=90 °C**	**19** **NaOH :31.25 mmol/L** **$Zn(NO_3)_2$： 225 mmol/L** **V=12.5 mL/min** **T=90 °C**	**20** **NaOH : 0 mmol/L** **$Zn(NO_3)_2$： 300 mmol/L** **V=12.5 mL/min** **T=90 °C**
21 **NaOH :125 mmol/L** **$Zn(NO_3)_2$： 0 mmol/L** **V=5 mL/min** **T=90 °C**	**22** **NaOH :93.75 mmol/L** **$Zn(NO_3)_2$： 15 mmol/L** **V=5 mL/min** **T=90 °C**	**23** **NaOH :62.5 mmol/L** **$Zn(NO_3)_2$： 30 mmol/L** **V=5 mL/min** **T=90 °C**	**24** **NaOH :31.25 mmol/L** **$Zn(NO_3)_2$： 45 mmol/L** **V=5 mL/min** **T=90 °C**	**25** **NaOH : 0 mmol/L** **$Zn(NO_3)_2$： 60 mmol/L** **V=5 mL/min** **T=90 °C**

Fig. S10 List of the synthetic parameters of the 25 screened samples.

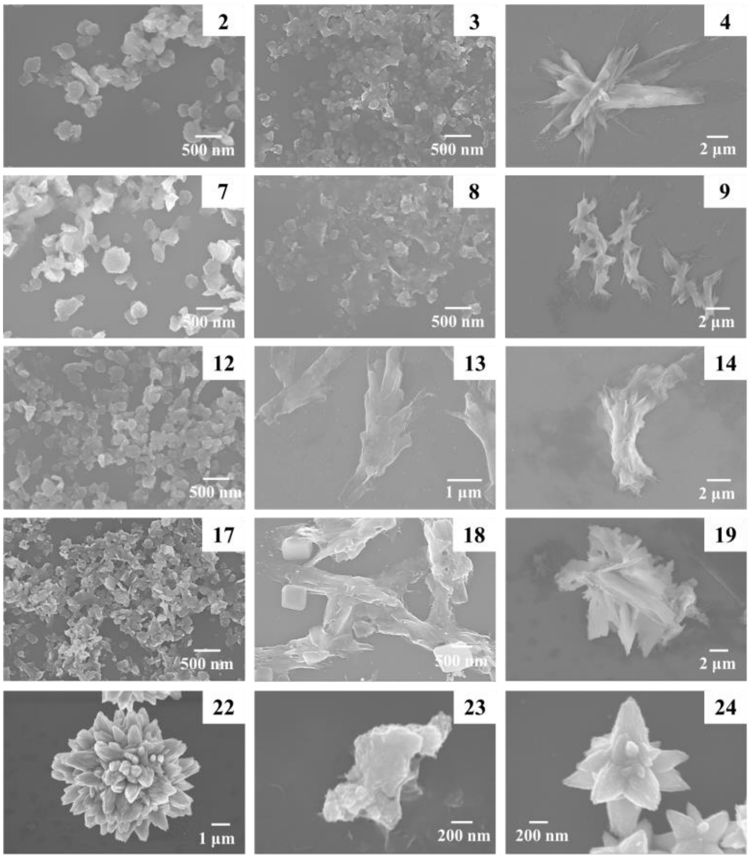

Fig. S11 SEM images of synthesized samples 2, 3, 4, 7, 8, 9, 12, 13 ,14, 17,18, 19, 22, 23 and 24 following the map in Fig. S9

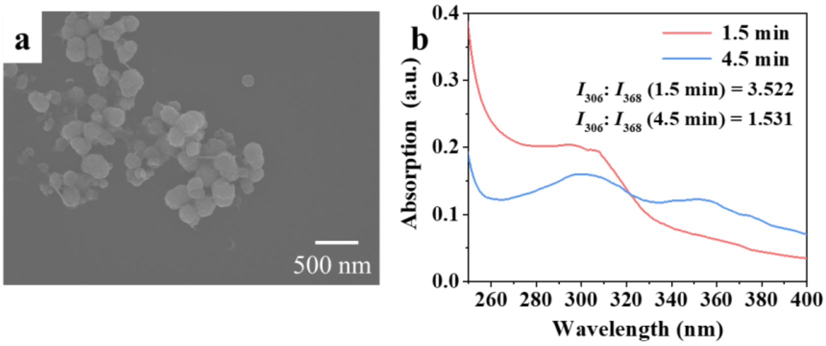

Fig. S12 (a) SEM image of the synthesized products in static experiments using similar concentrations of sample 24 after heating at 90°C for 4.5 min. (b) On-line spectra of synthesized products in static experiments using similar concentrations of sample 24 after heating at 90°C for 1.5 min and 4.5 min, respectively.

The static experiments were performed using similar concentrations of sample 24, and the obtained I_{306} to I_{368} ratios were found to be larger compared to those observed during online monitoring. This observation suggests that the reaction rate was lower in the static experiments compared to the flow synthesis process. Furthermore, SEM images of the samples showed smaller particle sizes, indicating an early stage of growth. These results revealed that the flow synthesis approach promotes faster reaction kinetics and allows for the control of particle size during the synthesis process.

As in flow chemistry, the continuous flow of reactants allows for precise control over reaction parameters such as temperature, residence time, and mixing efficiency. It results in different reaction kinetics compared to static experiments where reaction conditions might not be well-controlled. 3D microchannels offer enhanced mass and heat transfer due to the continuous flow of reactants and enhanced mixing, leading to improved reaction rates, uniformity, and control over particle size and shape compared to static experiments, where mass and heat transfer may be limited. This 3D configuration offers a compact device design, and provides more concentration combinations owing to two layers of CGGs and high spatiotemporal resolution of spectroscopic monitoring, which will pave the way for advanced prototyping of 3D glass-based autonomous continuous-flow “factory-on-a-chip” microsystems with intelligent feedback control.

References:

[1] S. Marre, K. F.Jensen, Chem. Soc. Rev., 2010, 39, 1183-1202

[2] K. S. Elvira, X. C. I. Solvas, R.C. R. Wootton and A. J. DeMello, Nat. Chem., 2013, 5, 905-915

[3] R. Munirathinam, J. Huskens, and W. Verbooma, Adv. Synth. Catal., 2015, 357, 1093 –1123

[4] Y. Xu, D.-Y. Zhang, X.-Y. Meng, X. Liu, S. Sheng, G.-H. Wu, J. Wang, F.-A. Wu, J. Pharm. Biomed. Anal., 2017, 137, 243–251

[5] Y. Liu and X. Y. Jiang, Lab Chip, 2017, 17, 3960-3978